Metallic and Semiconducting Single-Walled Carbon Nanotubes: Differentiating Individual SWCNTs by Their Carbon 1s Spectra

David Rossouw,[†] Gianluigi A. Botton,[†,‡] Ebrahim Najafi,[‡,§,⊥] Vincent Lee,[‡,§] and Adam P. Hitchcock[‡,§,*]

[†]Department of Materials Science and Engineering, McMaster University, Hamilton, ON, Canada, L8S4M1, [‡]Brockhouse Institute for Materials Research, McMaster University, Hamilton, ON, Canada L8S 4M1, and [§]Department of Chemistry & Chemical Biology, McMaster University, Hamilton, ON, Canada L8S4M1. [⊥]Present address: Chemical Physics, California Institute of Technology, Pasadena, Calilfornia 91125, United States.

ABSTRACT The C 1s inner shell excitation spectra of individual metallic and semiconducting single-walled carbon nanotubes (SWCNTs) were measured using high-resolution electron energy loss spectroscopy in an aberration-corrected transmission electron microscope (TEM-EELS). On the basis of its diameter, the metallic SWCNT is most likely a (10,10) sample, whereas (11,12) and a number of other chiral vectors are consistent with the diameter of the semiconducting SWCNTs. The C 1s X-ray absorption spectra of the same electronically pure SWCNT materials were measured as individual bundles or agglomerations of bundles by scanning transmission X-ray microscopy. Spectral differences in the C 1s → π^* transitions of metallic and semiconducting species, related to differences in the van Hove singularities in their unoccupied states, are observed by both methods. The fine structure of the C 1s → π^* transitions is similar to that recently reported from nonspatially resolved X-ray absorption spectroscopy of ensemble samples of high-purity metallic and semiconducting SWCNTs. The quality of the TEM-EELS spectra of individual SWCNTs is such that the line shape can be used to identify if they are metallic or semiconducting, thereby opening up the possibility to interrogate the electronic state of single-SWCNT devices. A strong X-ray linear dichroism in the C 1s → π^* band of both types of SWCNTs was observed.

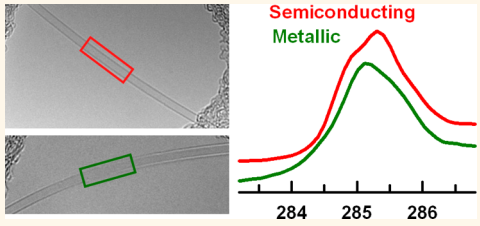

KEYWORDS: chiral single-walled carbon nanotubes · metallic · semiconducting · EELS · TEM · near edge X-ray absorption spectroscopy · scanning transmission X-ray microscopy

Single-walled carbon nanotubes (SWCNTs) are ideal candidates for building miniature electronic devices owing to their unique electronic structure and large aspect ratio.[1] However, practical advances have been relatively slow mainly because economic methods for producing chemically and chirally pure SWCNTs are not yet available. Current high-volume synthetic processes yield a blend of semiconducting and metallic SWCNTs with variable chirality and diameter. Separation techniques such as agarose gel chromatography,[2] alternating current assisted dielectrophoresis,[3] and density gradient ultracentrifugation (DGU)[4,5] are frequently used to separate SWCNTs by their electronic structure at the laboratory scale. Development of the DGU method has recently led to commercial availability of high-purity metallic and semiconducting SWCNTs.[6] While not chirally specific, the samples have a very narrow range of diameter and a very pure electronic character. By examining individual tubes from these samples, it is thus practical to measure the spectra, and thus electronic structure, of chirally specific samples. Purified SWCNTs are often evaluated by UV−visible,[7] Raman,[5] or near-infrared photoluminescence spectroscopies.[8] While such spectroscopic techniques successfully characterize SWCNT powders, they lack the spatial resolution needed to investigate individual or bundles of SWCNTs.

The electronic conductivity of SWCNTs is dependent on the chirality and diameter. This is due to the quantization of the wave vector around their circumference, which allows only a subset of states in the Brillouin zone of graphene from which SWCNTs are constructed. Similar to graphene, where the metallic conductivity is induced by degenerate states at the *K*-point in the Brillouin

* Address correspondence to aph@mcmaster.ca.

Received for review September 29, 2012 and accepted November 25, 2012.

Published online November 25, 2012
10.1021/nn3045227

zone, SWCNTs are metallic only if the *K*-point is contained in the set of allowed states; otherwise SWCNTs are semiconducting.[9−11]

Inner shell spectra, measured by electron energy loss spectroscopy (EELS) in a modern analytical transmission electron microscope (TEM-EELS)[12] or by near edge X-ray absorption spectroscopy (NEXAFS)[13] in an analytical scanning transmission X-ray microscope (STXM),[14,15] are frequently used to examine the electronic structure of materials. Inner shell spectra provide an atom-localized and symmetry-projected sampling of the unoccupied electronic states. High-resolution NEXAFS spectroscopy of SWCNT powders shows fine structure in the C 1s → π^* transition,[16−20] which is due to transitions to van Hove singularities in the unoccupied states. Several theoretical treatments of this fine structure[17−21] have been presented, and a consensus view of the spectral interpretation is emerging. Recently we have used TEM-EELS and STXM-NEXAFS to investigate the physical and chemical properties of CNTs, including structural order, by monitoring the electron[22] and X-ray linear dichroism[23−25] at the C 1s → π^* transition. Here, we have used TEM-EELS and STXM to measure the C 1s spectra of metallic and semiconducting SWCNTs at high energy and spatial resolution. We show that the fine structure in the π^* peak can be measured from individual bundles with STXM-NEXAFS and even from a single SWCNT, in the case of TEM-EELS. This opens up the possibility to interrogate the electronic state of single-SWCNT devices.

RESULTS

Optical Spectroscopy. Figure 1a is a photograph of the metallic and semiconducting SWCNTs dissolved in *N*,*N*-dimethylformamide. The solution with metallic SWCNTs is green, while the solution with semiconducting SWCNTs is red. These solutions remained clear with a similar color intensity for several weeks after the samples were prepared. After several months the solution color faded somewhat and some suspended black particles were observed. Figure 1b presents optical spectra of DMF solutions of the metallic and semiconducting SWCNT samples. The color change and the spectra are fully consistent with the metallic SWCNT sample having a spectrum (green line) dominated by the M_{11} band, while the semiconducting SWCNT has a spectrum (red line) dominated by the S_{22} band, in each case the features known to be characteristic of metallic and semiconducting SWCNTs, respectively.[8] The purity is evidenced by the low levels of signal at the M_{11} band position in the semiconducting sample and at the S_{22} band position in the metallic sample.

C 1s Spectroscopy. Figure 2a and b presents high-resolution TEM images of individual semiconducting and metallic SWCNTs, respectively. Careful measurements

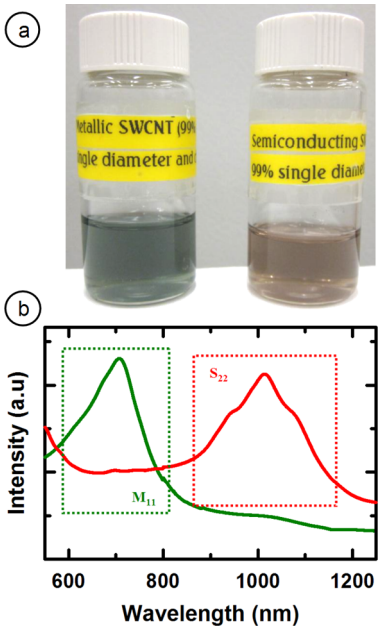

Figure 1. (a) Photographs of DMF solutions of metallic (left, green) and semiconducting (right, red) SWCNTs. (b) Optical (visible and near-infrared) spectra of metallic (green line) and semiconducting (red line) SWCNTs measured in DMF.

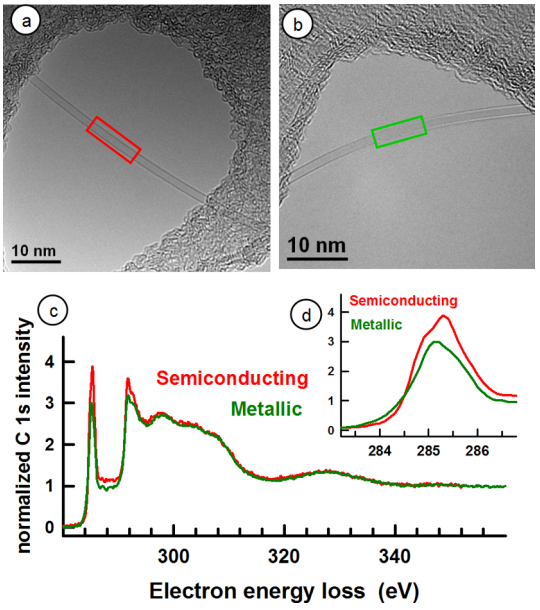

Figure 2. (a) Bright-field, high-resolution transmission electron microscope (HR-TEM) image of a metallic SWCNT (A) suspended from lacey carbon. (b) HR-TEM image of a semiconducting SWCNT suspended from lacey carbon. In (a) and (b) the rectangles indicate the region from which C 1s spectra were recorded using spectral imaging. (c) C 1s spectra of the metallic and semiconducting SWCNTs. The EELS spectra were calibrated using the NEXAFS results. A curved background extrapolated from the pre-C 1s region was subtracted, and the intensity at 360 eV normalized to 1. (d) Expansion of (c) in the region of the C 1s → π^* band.

of the diameter of the SWCNT in the region where the spectra were recorded determined the diameters to be 1.35(1) nm for the metallic SWCNT and 1.56(3) nm for the

TABLE 1. Peak Positions (eV) and Assignments for Spectral Features in the C 1s Spectra of Semiconducting and Metallic SWCNTs

semiconducting SWCNT		metallic SWCNT		
TEM-EELS	NEXAFS	TEM-EELS	NEXAFS	assignment
284.9 (sh)	284.9	284.4 (sh)	284.5	π^*
(285.33)	285.33[a]	(285.15)	285.15[b]	π^*
285.9 (sh)	285.8	285.6 (sh)	285.6	π^*
291.74	291.66	291.77	291.68	σ^* exciton
292.6	292.6	293.0	292.9	σ^* band
297.6	298.2	298.0	298	σ^* band
303	303	304	304	σ^* band
307 (sh)	307	308 (sh)	308	σ^* band
327.4		328.1		σ^* band

[a] Calibrated relative to CO_2 3p ($v = 0$) Rydberg line (−9.63(3) eV). [b] Calibrated relative to CO_2 3p ($v = 0$) Rydberg line (−9.81(3) eV).

semiconducting SWCNT. The diameter for the metallic sample is consistent with chiral indices of (10,10) (predicted diameter of 1.36 nm), while the diameter for the semiconducting sample is consistent with a number of chiral indices with best fit to (11,12) (d_{pred} = 1.56 nm) but also compatible with chiral indices of (7,15), d_{pred} = 1.52 nm; (6,16), d_{pred} = 1.54 nm; (9,14), d_{pred} = 1.57 nm; and (8,15), d_{pred} = 1.58 nm. Note the indicated uncertainty is a precision, based on our ability to measure tube diameters from HR-TEM images. Systematic errors as large as 5% of the spatial scale could exist, which would bring into range two other possible chiral indices of the metallic SWCNT: (11,8) with a diameter of 1.29 nm and (13,7) with a diameter of 1.38 nm. Figure 2c compares C 1s electron energy loss spectra measured using spectral imaging (EELS spectrum recorded at each pixel) from the regions of each SWCNT indicated by the rectangular boxes in Figure 2a and b. The energy scale was calibrated using the NEXAFS data (see Table 1). The pre-edge signal was extrapolated and subtracted to isolate the signal solely from C 1s excitation and ionization. The intensity at 360 eV was set to 1. The raw spectra exhibit a very weak pre-C 1s intensity, consistent with the level observed in the X-ray absorption spectra, indicating there is negligible plural scattering, as expected from the extremely thin sample. The C 1s spectra of the two types of SWCNTs are very similar, essentially overlapping, except for small differences in the 283−296 eV region. Figure 2d is an expanded presentation of the spectra in the region of the C 1s → π^* peak. A clear difference between the metallic and semiconducting SWCNTs is observed in the shape and intensity (relative to the far continuum) of the C 1s → π^* peak.

Figure 3a presents the HR-TEM image of a second metallic SWCNT (labeled B) on the same grid as metallic SWCNT A in Figure 2a. Figure 3b is the small-area electron diffraction (ED) signal of metallic SWCNT B, recorded with a beam size approximately 25 nm in diameter that sampled most of SWCNT B in the hole in

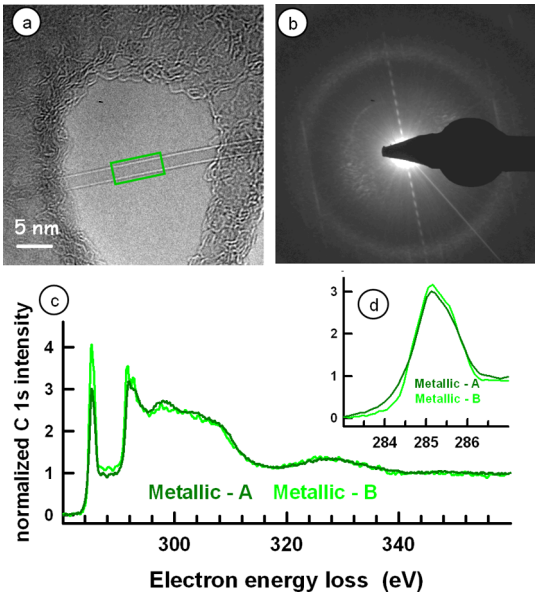

Figure 3. (a) Bright-field, HR-TEM image of metallic SWCNT (B), a different SWCNT on the same grid as metallic SWCNT A (Figure 2). The rectangle indicates the region from which the spectrum was measured using spectral imaging. (b) Electron diffraction pattern recorded from metallic SWCNT B with a parallel beam approximately 25 nm in diameter. (c) C 1s EELS spectra of metallic SWCNT B compared to that of A. The EELS spectra were processed as summarized in the caption to Figure 2. (d) Comparison of the rescaled C 1s EELS spectra of metallic SWCNTs A and B in the region of the C 1s → π^* band.

the lacy carbon. Interpretation of the ED pattern according to the procedure of Gao *et al.*[26,27] indicates this tube has chiral indices of (16, 10), which would have a diameter of 1.78 nm. Direct measurement of the diameter from the image was complicated by the Fresnel fringes in the slightly defocused image. Averaging values from the inside and outside of the Fresnel fringes gave an estimated diameter of 2.0(3) nm, which is in agreement with the diameter deduced from the ED, within the error estimate. Figure 3c presents the TEM-EELS spectrum of metallic SWCNT B in comparison to that of A. Outside the π^* and σ^* region the spectra are very similar. However that of B is relatively more intense throughout the 284 to 292 eV region, and the 291.8 eV σ^* exciton is considerably more pronounced. It is possible this difference reflects the presence of some residual surfactant and DGU agents in SWCNT A. Figure 3d compares the shape of the C 1s → π^* peaks of A and B. After rescaling the peaks are remarkably similar.

Figure 4a and b presents STXM images of semiconducting and metallic SWCNTs, respectively. For each STXM image there is an inset TEM image of the same region. The C 1s spectra extracted from the regions highlighted in Figure 4a and b are plotted in Figure 4c. The measured spectra were calibrated relative to the sharp C 1s → 3p ($v = 0$) Rydberg line of gaseous CO_2 recorded shortly after the SWCNT measurement.

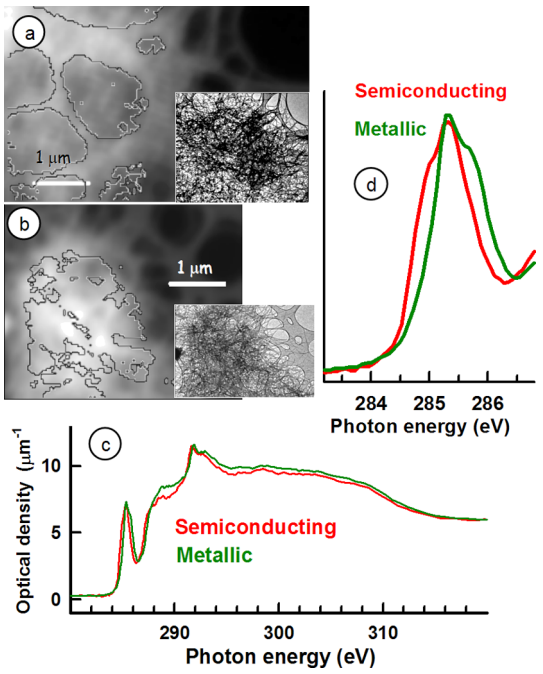

Figure 4. (a) Sum of all OD images in the image sequence of an assembly of metallic SWCNTs suspended from lacey carbon. [OD image = recorded transmission image, converted to optical density, OD, where OD = $-\ln(I/I_o)$; I_o is taken from the signal in a hole.] (b) Sum of all OD images in the image sequence of an assembly of semiconducting SWCNTs suspended from lacey carbon. The inset images in (a) and (b) are TEM bright-field images of the same area. The gray lines in (a) and (b) indicate the boundaries of the regions (within holes in the lacey carbon support) that were averaged to obtain the spectra. (c) C 1s X-ray absorption spectra of the metallic and semiconducting SWCNTs. The recorded data have been scaled to match the predicted spectrum of elemental carbon (d = 1.5 g/cm^3) below 282 eV and above 318 eV.[28] (d) Expansion of Figure 4c in the region of the C 1s → π* band.

The intensity was scaled so as to match the optical density of the 1 nm thickness of elemental carbon at a density of 1.5 g/cm^3 in the regions below 283 eV and above 316 eV.[28] As with the TEM-EELS data, the spectra of the metallic and semiconducting SWCNTs are very similar to each other. However the NEXAFS spectra differ significantly from the TEM-EELS data, especially above 287 eV. This is due to the presence of impurities, mainly sodium dodecyl sulfate (SDS, an aliphatic surfactant) and sodium cholate (the density gradient material), despite much effort to remove these materials by various solvent extraction and annealing methods. Since aliphatic materials such as SDS and sodium cholate do not have C 1s spectral features below 287 eV,[29] the presence of these impurities does not impact our observations of the C 1s → π* band. Figure 4d is an expanded presentation of Figure 3c in the region of the C 1s → π* band. Clear spectral differences are observed, and the general character of these differences is very similar to that observed in the TEM-EELS spectra (Figure 2).

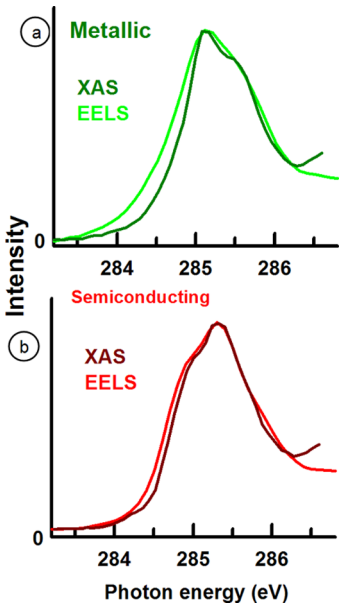

Figure 5. Comparison of the C 1s → π* band for metallic and semiconducting SWCNTs measured by X-ray absorption and electron energy loss spectroscopy. The EELS spectrum is that of metallic SWCNT tube A. The rise in the NEXAFS data above 286.5 eV is due to the presence of SDS and sodium cholate impurities in the NEXAFS sample.

Figure 5 presents a direct comparison of the TEM-EELS and STXM-NEXAFS spectra of the metallic and semiconducting SWCNTs in the region of the C 1s → π* band. The fine features are somewhat clearer and the overall bandwidth slightly narrower in the NEXAFS spectra due to its somewhat better energy resolution, but otherwise the NEXAFS and EELS spectra of the same material are remarkably similar to each other. The energies of the spectral features in both the TEM-EES and NEXAFS spectra are summarized in Table 1. We note that, in contrast to the TEM-EELS case, where the spectrum truly is from one single, chiral SWCNT, the NEXAFS spectra are from an aggregation of randomly oriented bundles of SWCNTs, most likely consisting of tubes with a range of diameters. The EELS and NEXAFS spectra have the same overall shapes, but the full width at half-maximum of the NEXAFS peak is slightly narrower. They are also in very good agreement with other, recently published nonspatially resolved spectra of DGU-purified metallic and semiconducting SWCNTs,[17−20] which are unlikely to have the same mixture of chiral species. This suggests the electronic character—metallic *versus* semiconducting—is the critical determiner of the spectral shape and that averaging over a range of diameters, and thus chiralities, and lengths of SWCNTs does not significantly broaden or otherwise alter the shape of the C 1s → π* band. This perspective is supported by the excellent agreement in π* spectral shape of metallic SWCNTs A and B (see Figure 3d), despite the fact they have significantly different diameters and thus chiral indices.

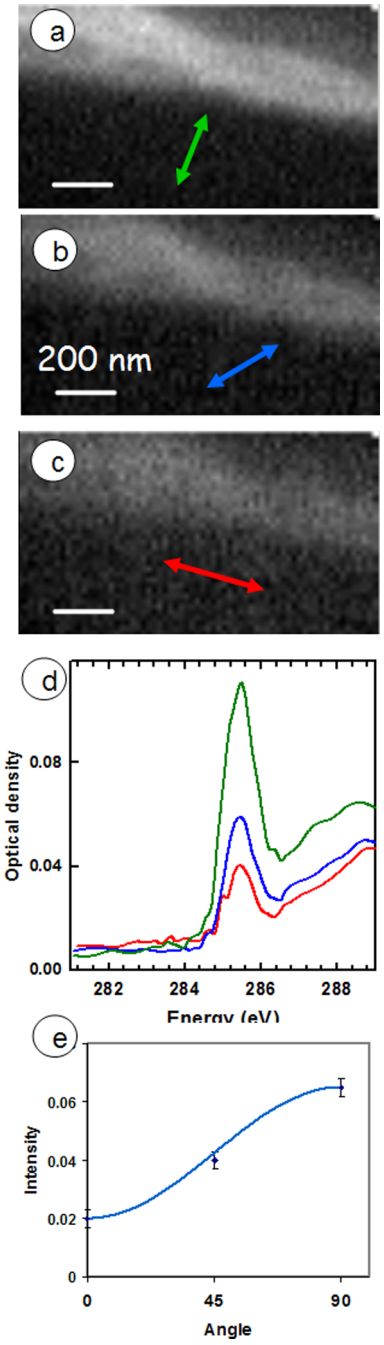

Figure 6. (a–c) Images of an individual semiconducting SWCNT bundle averaged over 284–287 eV (the C 1s → π^* band) measured with E-vector oriented at 90°, 45°, and 0° relative to the long axis of the SWCNT bundle, respectively. The double-headed arrow indicates the E-vector orientation (d) C 1s spectra averaged over the whole bundle for each E-vector orientation. (e) Peak area (points) compared to the expected $\cos^2(\theta)$ intensity distribution for X-ray linear dichroism.

Dichroism at the C 1s → π^* Band. Early TEM-EELS studies of carbon nanotubes[30,31] had detected a sizable difference of the C 1s spectrum of the edge and center of MWCNTs, but had suggested there would be little difference in the spectrum with polarization across *versus* along SWCNTs, particularly those with small diameters, due to the high curvature and thus expected large $\pi-\sigma$ mixing. Recently we had found a surprisingly large across/along dichroism in the XAS of bundles of SWCNTs[25] and wished to see if these very high-quality electronically pure SWCNTs also had a strong dichroism. Figure 6a–c displays images recorded at 285.3 eV of the same region of an isolated bundle of semiconducting SWCNTs recorded with the E-vector aligned (a) parallel, (b) at 45°, and (c) perpendicular to the long axis of the SWCNT. The orientation of the E-vector relative to the long axis of the bundle of semiconducting SWCNTs is indicated by an arrow. Figure 6d presents the C 1s spectra for each situation, in each case averaged over the areas displayed. Although the shape remains the same, the intensity of the C 1s → π^* transition changes significantly with E-vector orientation. Figure 6e is a plot of the integrated peak intensity as a function of θ, the angle between the E-vector and the long axis of the semiconducting SWCNT bundle. The good agreement with the expected $\cos^2(\theta)$ relationship[14] indicates the intensity variation is the linear dichroism for this transition. The complex line shape arises since each symmetry unique site in the SWCNT has a different C 1s → π^* transition. The fact that the peak shape is independent of θ indicates that all the subtransitions making up this line shape have the same symmetry. In principle the intensity of the C 1s → π^* transition should be 0 when the E-vector is 100% linearly polarized and aligned along the long axis of a perfect carbon nanotube. Three reasons may explain the nonzero intensity at $\theta = 0$, indicated in Figure 6e. First, the region where the spectra were acquired is not a single SWCNT but rather a bundle, and there is a range of orientations of the CNTs (see Figure 6a–c). Second, the polarization is not 100%; there is ~10% of circularly polarized light at 285 eV due to the effect of graphitic impurities on the optical surfaces of the beamline. Third, as shown earlier,[23–25] the presence of structural defects reduces the dichroic signal. Despite these factrs, it is clear that small-diameter semiconducting SWCNTs exhibit a large across/along dichroic response, as was previously shown to be characteristic of high-quality (low defect content) SWCNTs[25] as well as MWCNTs.[23,24] The metallic SWCNTs showed a similar linear dichroic response (not shown). This suggests that the purification and chiral selection processes preserved the structural integrity of the tubes.

DISCUSSION

The C 1s → π^* peaks in the spectra of metallic and semiconducting SWCNTs show distinct differences. The metallic sample shows a sharp peak at 285.13(4) eV and a high-energy shoulder at 285.54(8) eV, whereas the semiconducting sample shows a sharp peak at 285.33(4) eV and a low-energy shoulder at 284.9(1) eV. These fine structures correspond to transitions to van

Hove singularities in the unoccupied density of states,[16−21] which differ for metallic and semiconducting SWCNTs.[8−11] The smaller peak width for the metallic SWCNTs (full width at half-maximum, fwhm = 0.80 eV) than that for the semiconducting SWCNTs (fwhm = 1.02 eV) suggests a closer spacing between van Hove singularities in the metallic sample. The natural line width determined by the core hole lifetime is less than 0.1 eV for C 1s excited states.[32] Instrumental broadening in both the TEM-EELS and STXM-NEXAFS was less than 0.1 eV. Thus, these widths are a clear indication of the multistate character of these features.

Mowbray *et al.*[20] have reported advanced calculations of the C 1s spectrum of a (10,10) metallic SWCNT, which is most likely the chiral indices of the metallic SWCNT that was measured by TEM-EELS (Figure 2). Their calculation predicts a structured π^* peak with a high-energy shoulder of somewhat lower intensity than the main peak (see Figure 3 of ref 21). While the shape of their calculated spectrum is in qualitative agreement with experiment, the separation of the two main components is predicted to be 0.80 eV, whereas our experimental result indicates a separation of 0.45 eV (in agreement with other experimental results[17−20]), and the main peak in the computed spectrum is lower than the main peak in the experimental spectrum by 0.21 eV. Thus, while these latest calculations are much closer to experiment than earlier results,[21] further improvements to the calculations are needed to have a method that will predict accurately the C 1s spectra of specific chiral SWCNTs.

SUMMARY

TEM-EELS was used to measure the C 1s spectra of individual metallic and semiconducting SWCNTs and shown to be of comparable spectral resolution and quality to NEXAFS spectra of the same material. While overall features in the C 1s spectra of these samples were similar, significant differences between the metallic and semiconducting species were observed in the fine structure of the C 1s $\rightarrow \pi^*$ peak. The fine structure was similar to that reported previously in non spatially resolved NEXAFS studies.[17−20] The fine structure can be used to identify the electronic character of individual SWCNTs.

METHODS

Sample Preparation. The samples used for this study were highly purified metallic and semiconducting SWCNTs with stated diameter ranges of 1.2−1.7 nm.[33] The raw SWCNTs were made by arc discharge and further purified according to their chirality and diameter using DGU, which uses structure-discriminating surfactants to induce subtle differences in the buoyant density of SWCNTs. The SWCNTs were then separated by ultracentrifugation to achieve >99.9 wt % chirality and diameter purity.[4,6] Although nearly completely separated into metallic and semiconducting samples, as determined by their visible spectra (see Figure 1), the samples do consist of SWCNT with a range of diameters (1.2−1.7 nm), which correspond to a range of different chiral indices.

Samples for STXM measurements were prepared by dispersing SWCNTs in *N*,*N*-dimethylformamide (DMF) using ultrasonication. The samples were sonicated for less than two minutes to minimize modification of their chemical, physical, and electronic properties.[34] The solutions were then drop cast onto holey carbon grids. The grids were left to air-dry overnight and then further dried in a vacuum oven for 7 days at 200 °C. For some measurements, samples were also purified by heating to 400 °C in air for 24 h.

The samples used for TEM-EELS measurements were the same as those prepared for STXM; in fact, in several cases exactly the same area of the same grid was examined by both techniques. For the TEM-EELS measurements, however, additional removal of the SDS and sodium cholate impurities was achieved by heating the sample in the electron microscope. STXM measurements of the same grids used for TEM measurements were made a few weeks later, but all STXM measurements showed significant interference from the SDS and cholate impurities. We suspect the SDS and cholate impurities are mobile and recontaminate the SWCNT in a short time.

Transmission electron Microscopy−electron Energy Loss Spectroscopy. TEM-EELS images and spectra were measured using a FEI Titan 80-300 Cubed microscope operated in scanning TEM (STEM) mode at 80 kV to minimize knock-on damage. This microscope is equipped with a high-brightness field emission gun and a Wien-type monochromator to reduce chromatic aberration of the electron beam and to improve the energy resolution. The spectra were recorded in parallel detection mode using a postcolumn Gatan Tridiem 866 high-resolution imaging filter. The energy resolution was 63 meV, as measured at the zero-loss peak (fwhm). The dwell time for spectral acquisition at each spatial pixel was 0.5 s. The convergence angle of the incident beam and collection angle of the scattered beam for the measurements were 6 and 12 mrad, respectively. These conditions are such that effects of electron linear dichroism are minimal,[22,35] and thus the C 1s spectra are expected to be very similar (in terms of relative intensities of spectral features and absence of dichroism) to the C 1s NEXAFS that would be measured using circularly polarized X-rays or from a collection of randomly oriented SWCNTs.

Transmission Electron Microscopy−Electron Diffraction. Small-area electron diffraction patterns were measured using the same FEI Titan 80-300 Cubed microscope operated in nanoprobe mode at 80 kV. A 10 μm condenser aperture was used to limit the approximately parallel beam to 25 nm in diameter, enabling ED measurements from an isolated SWCNT. The chiral indices (*u*,*v*) of the SWCNT were determined by distance measurements between the first-order graphite-like streaks in the diffraction pattern and the equatorial line crossing the origin (according to Gao *et al.*[26]). On the basis of the three distance measurements we measure a chiral angle of 22.5° and a *v*/*u* ratio of 0.629. These values match those of a (16,10) nanotube within experimental error.

Scanning Transmission X-ray Microscopy−X-ray Absorption Spectroscopy. In STXM, a monochromated beam of X-rays is focused to 30 nm by a Fresnel zone plate; the sample is then raster scanned though the focal spot while transmitted X-rays are recorded. C 1s spectral image sequences were measured by recording 200 images over photon energies between 278 and 320 eV. The measured image sequences were aligned, then converted to optical density using the incident flux (I_o) spectrum recorded simultaneously in areas next to the bundled SWCNT. STXM measurements were conducted at two different facilities. Beamline 5.3.2.2 at the Advanced Light Source (ALS, Berkeley, CA, USA)[36,37] is a bend magnet beamline for which the X-rays are in-plane (horizontal) linear polarized with a degree of polarization

at the C 1s edge measured to be ~85%.[38] The 10ID1 beamline at the Canadian Light Source (CLS, Saskatoon, SK, Canada)[39] is equipped with an elliptically polarizing undulator with four movable quadrants, thereby allowing full control of the spatial orientation of the E-vector. In addition to providing confirmatory spectral data, the CLS measurements were used to explore the linear dichroism of the C 1s → π^* transitions of the metallic and semiconducting SWCNTs.

Conflict of Interest: The authors declare no competing financial interest.

Acknowledgment. This research was supported by NSERC (Discovery Grants to A.P.H. and G.A.B.), CFI, and the Canada Research Chair program. Electron microscopy was performed at the Canadian Centre for Electron Microscopy (CCEM), which is a Canadian national facility supported by NSERC and McMaster University. STXM was performed at the Advanced Light Source (ALS) and the Canadian Light Source (CLS). ALS is supported by the Director, Office of Energy Research, Office of Basic Energy Sciences, Materials Sciences Division of the U.S. Department of Energy, under Contract No. DE-AC02-05CH11231. CLS is supported by NSERC, CIHR, NRC, the Province of Saskatchewan, WEDC, and the University of Saskatchewan.

REFERENCES AND NOTES

1. Baughman, R. H.; Zakhidov, A. A.; de Heer, W. A. Carbon Nanotubes—the Route Toward Applications. *Science* **2002**, *297*, 787–792.
2. Zheng, M.; Semke, D. Enrichment of Single Chirality Carbon Nanotubes. *J. Am. Chem. Soc.* **2007**, *129*, 6084–6085.
3. Krupke, R.; Hennrich, F.; von Lohneysen, H.; Kappes, M. M. Separation of Metallic from Semiconducting Single-Walled Carbon Nanotubes. *Science* **2003**, *301*, 344–347.
4. Arnold, M. S.; Green, A. A.; Hulvat, J. F.; Stupp, S. I.; Hersam, M. C. Sorting Carbon Nanotubes by Electronic Structure Using Density Differentiation. *Nat. Nanotechnol.* **2006**, *1*, 60–65.
5. Miyata, Y.; Yanagi, K.; Maniwa, Y.; Kataura, H. Optical Evaluation of the Metal-to-Semiconductor Ratio of Single-Wall Carbon Nanotubes. *J. Phys. Chem. C* **2008**, *112*, 13187–13191.
6. Hersam, M. C. Progress Towards Monodisperse Single-Walled Carbon Nanotubes. *Nat. Nanotechnol.* **2008**, *3*, 387–394.
7. Kim, W. J.; Usrey, M. L.; Strano, M. S. Selective Functionalization and Free Solution Electrophoresis of Single-Walled Carbon Nanotubes: Separate Enrichment of Metallic and Semiconducting SWNT. *Chem. Mater.* **2007**, *19*, 1571–1576.
8. Berciaud, S.; Cognet, L.; Poulin, P.; Weisman, R. B.; Lounis, B. Absorption Spectroscopy of Individual Single-Walled Carbon Nanotubes. *Nano Lett.* **2007**, *7*, 1203–1207.
9. O'Connell, M. J. *Carbon Nanotubes: Properties and Applications*; CRC Press: Boca Raton, FL, 2006.
10. Jorio, A.; Dresselhaus, M.; G. Dresselhaus, G. *Carbon Nanotubes: Advanced Topics in the Synthesis, Structure, Properties and Applications*; Springer-Verlag: Heidelberg, Germany, 2008.
11. Guldi, D. M.; Martin, N. *Carbon Nanotubes and Related Structures*; Wiley-VCH: Weinheim, Germany, 2010.
12. Egerton, R. F. *Electron Energy-Loss Spectroscopy in the Electron Microscope*, 3rd ed.; Springer: Berlin, Germany, 2011.
13. Stöhr, J. *NEXAFS Spectroscopy*; Springer-Verlag: Berlin, 1992.
14. Ade, H.; Hitchcock, A. P. NEXAFS Microscopy and Resonant Scattering: Composition And Orientation Probed in Real and Reciprocal Space. *Polymer* **2008**, *49*, 643–675.
15. Hitchcock, A. P. In *Handbook on Nanoscopy*; Van Tendeloo, G., Van Dyck, D., Pennycook, S. J., Eds.; Wiley: New York, 2012; Vol. II, Chapter 22, Soft X-ray Imaging and Spectromicroscopy, pp 745–791.
16. Kramberger, C.; Rauf, H.; Shiozawa, H.; Knupfer, M.; Büchner, B.; Pichler, T. Unraveling Van Hove Singularities in X-Ray Absorption Response of Single-Wall Carbon Nanotubes. *Phys. Rev. B* **2007**, *75*, 235437-(1–4).
17. Ayala, P.; Miyata, Y.; De Blauwe, K.; Shiozawa, H.; Feng, Y.; Yanagi, K.; Kramberger, C.; Silva, S. R. P.; Follath, R.; Kataura, T. Disentanglement of the Electronic Properties of Metallicity-Selected Single-Walled Carbon Nanotubes. *Phys. Rev. B* **2009**, *80*, 205427-(1–6).
18. Ayala, P.; Shiozawa, H.; De Blauwe, K.; Miyata, Y.; Follath, R.; Kataura, H.; Pichler, T. An X-Ray Absorption Approach to Mixed and Metallicity-Sorted Single-Walled Carbon Nanotubes. *J. Mater. Sci.* **2010**, *45*, 5318–5322.
19. De Blauwe, K.; Mowbray, D. J.; Miyata, Y.; Ayala, P.; Shiozawa, H.; Rubio, A.; Hoffmann, P.; Kataura, H.; Pichler, T. Combined Experimental and *Ab Initio* Study of the Electronic Structure of Narrow-Diameter Single-Wall Carbon Nanotubes with Predominant (6,4),(6,5) Chirality. *Phys. Rev. B* **2010**, *82*, 125444.
20. Mowbray, D. J.; Ayala, P.; Pichler, T.; Rubio, A. Computing C1s X-ray Absorption for Single-Walled Carbon Nanotubes with Distinct Electronic Type. *Mater. Express* **2011**, *1*, 225–230.
21. Gao, B.; Wu, Z.; Ågren, H.; Luo, Y. Chirality and Diameter Dependent X-Ray Absorption of Single Walled Carbon Nanotubes. *J. Chem. Phys.* **2009**, *131*, 034704-(1–7).
22. Najafi, E.; Hitchcock, A. P.; Rossouw, D.; Botton, G. Mapping Defects in a Carbon Nanotube by Momentum Transfer Dependent Electron Energy Loss Spectromicroscopy. *Ultramicroscopy* **2012**, *113*, 158–164.
23. Najafi, E.; Hernández Cruz, D.; Obst, M.; Hitchcock, A. P.; Douhard, B.; Pireaux, J. J.; Felten, A. Polarization Dependence of Tthe C 1s X-Ray Absorption Spectra of Individual Multi-Walled Carbon Nanotubes. *Small* **2008**, *4*, 2279–2285.
24. Felten, A.; Gillon, X.; Gulas, M.; Pireaux, J. J.; Ke, X.; Van Tendeloo, G.; Bittencourt, C.; Kilcoyne, A. L. D.; Najafi, E.; Hitchcock, A. P. Measuring Point Defect Density in Individual Carbon Nanotubes Using Polarization-Dependent X-ray Microscopy. *ACS Nano* **2010**, *4*, 4431–4436.
25. Najafi, E.; Wang, J.; Hitchcock, A. P.; Guan, J.; Dénommée, S.; Simard, B. Characterization of Single-Walled Carbon Nanotubes by Scanning Transmission X-ray Spectromicroscopy: Purification, Order and Dodecyl Functionalization. *J. Am. Chem. Soc.* **2010**, *132*, 9020–9029.
26. Gao, M.; Zuo, M.; Twesten, R. D.; Petrov, I.; Nagahara, L. A.; Zhang, R. Structure Determination of Individual Single-Wall Carbon Nanotubes by Nanoarea Electron Diffraction. *Appl. Phys. Lett.* **2003**, *82*, 2703–2705.
27. Qin, L.-C. Electron Diffraction from Carbon Nanotubes. *Rep. Prog. Phys.* **2006**, *69*, 2761–2821.
28. Henke, B. L.; Gullikson, E. M. Davis, J. C. X-ray Interactions: Photoabsorption, Scattering, Transmission, and Reflection at E=50–30000 eV, Z=1–92. *At. Data Nucl. Data Tables* **1993**, *54*, 181–342 (updated version: http://henke.lbl.gov/optical_constants/).
29. Hitchcock, A. P.; Ishii, I. Carbon K-Shell Excitation Spectra of Linear and Branched Alkanes. *J. Electron Spectrosc. Relat. Phenom.* **1987**, *42*, 11–26.
30. Botton, G. A.; Burnell, G.; Humphreys, C. J.; Yadav, T.; Withers, J. C. Microstructural and Electron Spectroscopic Characterization of Carbon Nanostructures and Nanotubes Produced Using Multimetal Catalysts. *J. Phys. Chem. Solids* **1997**, *58*, 1091–1102.
31. Stéphan, O.; Kociak, M.; Henrard, L.; Suenaga, K.; Gloter, A.; Tencé, M.; Sandré, E.; Colliex, C. Electron Energy-Loss Spectroscopy on Individual Nanotubes. *J. Electron Spectrosc. Relat. Phenom.* **2001**, *114–116*, 209–217.
32. Prince, K. C.; Vondráček, M.; Karvonen, J.; Coreno, M.; Camilloni, R.; Avaldi, L.; de Simone, M. A Critical Comparison of Selected 1s and 2p Core Hole Widths. *J. Electron Spectrosc. Relat. Phenom.* **1999**, *101–103*, 141–147.
33. The samples were ISOM-99-P and ISOS-99-P materials purchased in June 2011 from NanoIntegris (8025 Lamon Avenue, Suite 43, Skokie, IL 60077).
34. Moonoosawmy, K.; Kruse, P. To Dope or Not to Dope: The Effect of Sonicating Single-Wall Carbon Nanotubes in

Common Lab Solvents on Their Electronic Structure. *J. Am. Chem. Soc.* **2008**, *130*, 13417–13424.
35. Pennycook, S. J.; Colliex, C. Spectroscopic Imaging in Electron Microscopy. *MRS Bull.* **2012**, *37*, 13–18.
36. Warwick, T.; Ade, H.; Kilcoyne, A. L. D.; Kritscher, M.; Tyliszczak, T.; Fakra, S.; Hitchcock, A. P.; Hitchcock, P.; Padmore, H. A. A New Bend Magnet Beam Line for Scanning Transmission X-ray Microscopy at the Advanced Light Source. *J. Synchrotron Rad.* **2002**, *9*, 254–257.
37. Kilcoyne, A. L. D.; Tyliszczak, T.; Steele, W. F.; Fakra, S.; Hitchcock, P.; Franck, K.; Anderson, E. K.; Harteneck, B.; Rightor, E. G.; Mitchell, G.; *et al*. Interferometrically Controlled Scanning Transmission Microscopes at the Advanced Light Source. *J. Synchrotron Rad.* **2003**, *10*, 125–136.
38. Watts, B.; Ade, H. A Simple Method for Determining Linear Polarization and Energy Calibration of Focused Soft X-Ray Beams. *J. Electron Spectrosc. Relat. Phenom.* **2008**, *162*, 49–55.
39. Kaznatcheev, K. V.; Karunakaran, Ch.; Lanke, U. D.; Urquhart, S. G.; Obst, M.; Hitchcock, A. P. Soft X-ray Spectromicroscopy Beamline at the CLS: Commissioning Results. *Nucl. Instrum. Methods A* **2007**, *582*, 96–99.